공학석사학위논문

기동성 및 횡 안정성을 위한 역삼륜형 퍼스널 모빌리티 차량의 인휠 모터 제어기 설계

In-Wheel Motor Controller Design of Three Wheeled Personal Mobility Vehicle for Maneuverability and Lateral Stability

2019 년 2 월

서울대학교 대학원

기계항공공학부

이 성 현

기동성 및 횡 안정성을 위한 역삼륜형 퍼스널 모빌리티 차량의 인휠 모터 제어기 설계

In-Wheel Motor Controller Design of Three Wheeled Personal Mobility Vehicle for Maneuverability and Lateral Stability

지도교수 이 경 수

이 논문을 공학석사 학위논문으로 제출함

2018 년 10 월

서울대학교 대학원

기계항공공학부

이 성 현

이성현의 공학석사 학위논문을 인준함

2018 년 12 월

위 원 장 _____

부위원장 _____

위 원 _____

Abstract

In-Wheel Motor Controller Design of Three Wheeled Personal Mobility Vehicle for Maneuverability and Lateral Stability

Sunghyun Lee

School of Mechanical and Aerospace Engineering

The Graduate School

Seoul National University

This study proposes dynamic analysis and in-wheel motor control algorithm of three wheeled personal mobility vehicle considering maneuverability and lateral stability. A dynamic modeling of personal mobility vehicle is used to understand the characteristics of system, which presents strategy of motor control algorithm. Dynamic characteristics are demonstrated based on various driving scenario simulation. Considering dynamic characteristics, desired yaw rate is designed as a function of longitudinal velocity. Tracking desired yaw rate generates additional yaw moment which satisfies the purpose of improvement of maneuverability and stability along with longitudinal velocity. This additional yaw moment is distributed as differential torque command to each front right and left motor. Differential torque command is processed by torque saturation logic to prevent pitchover and longitudinal wheel slip. Numerical simulation results are presented with some specific driving scenario

using Matlab/Simulink package to analyze controller's performance. Also, after embedding motor control algorithm into test vehicle, various vehicle tests are performed to verify the performance of designed controller at different speed, road condition, and driving scenario. According to test results, radius of curvature is significantly reduced at low longitudinal speed, which implicates the improvement of maneuverability. Also, lateral acceleration is upper bounded to prevent lateral instability of vehicle at high speed. Pichover and longitudinal slip is also prevented by in-wheel motor control algorithm.

Keywords: Personal Mobility Vehicle, In-Wheel Motor Control, desired yaw rate, Maneuverability, Stability.

Student Number: 2016-25667

Contents

List of Figures

Nomenclature

r	Radius of front wheel
Ω	Wheel angular velocity
δ_i	Front steer angle of i wheel
V_x	Vehicle's longitudinal speed
V_y	Vehicle's lateral speed
l_f	Distance from center of mass to front wheel
l_r	Distance from center of mass to rear wheel
t_w	Half of distance from left to right front wheel
α_i	Tire slip angle of i wheel
a	Half of tire's contact patch
c_p	Tire stiffness coefficient
μ	Friction coefficient
I_w	Moment of inertia of wheel
I_z	Yaw moment of inertia of PMV
a_y	Lateral acceleration
ϕ	Rider's tilting angle
F_{z_i}	Tire vertical force of i wheel
γ	Yaw rate of PMV
ω	Wheel's angular velocity
M_z	Yaw moment

K_{base}	Base model's understeer gradient
$\hat{F}_{yf}$	Estimated front lateral force
$\hat{F}_{yr}$	Estimated rear lateral force
L	Distance from two front wheel's center to rear wheel
K	Sliding mode gain
φ	Chattering bound value
β	Wheel angular acceleration margin
p	Pitch angle of PMV
a_{x_upp}	Upper bound of longitudinal acceleration
a_{x_low}	Lower bound of longitudinal acceleration
M_{z_pre}	Present yaw moment
ΔT	Stepsize of estimator
d_i	Process noise of i-th state
$v(k)$	Measurement noise of k-step
$L(k)$	k-step's kalman gain

Chapter 1

Introduction

1.1 Research Background

As vehicle market increases, the number of vehicle has been enormously increased along the centuries. Although such complexity of transportation system has satisfied the mankind's desire for mobility, it also resulted in many kinds of social problems, such as air pollution, lack of parking lot, traffic congestion, etc. To cope with such problems, new concepts for mobility have been introduced [Gohl 06, Nakajima 12], which is called multi-model transportation. According to this multi- model transportation, there should exist different types of vehicles along the travel distance. Especially, when moving short distance, micro mobility can be substitute of conventional vehicles to move in city. This strategy can reduce the problems which has been induced due to relatively heavy vehicles [Hibbard 96].

Recently, personal mobility vehicle (PMV) has attracted vehicle market as a new type of mobility to reduce complexity of transportation such as Honda's U3-X, Toyota's i-REAL, and Segway's Segway [Nakajima 12]. However most researches of PMV system are mainly focused on mechanism design and

electronic component integration [Nakagawa 13]. As market size of PMV increases, issues related to control performance and safety are also main factors to satisfy the consumer's needs. For conventional vehicle safety control system, electronic stability control (ESC) system [Lie 06] has been developed to increase maneuverability and stability for various driving situations. Embedding ESC to PMV system can be a novel research area for improvement of safety control problems of PMV system. Based on dynamic characteristics of PMV system, upper level in-wheel motor control algorithm can supplements the shortcomings of present PMV system.

1.2 Research Overview

The dynamic modeling of three wheeled PMV system is introduced. Based on brush tire model, steering mechanism, and Newton-Euler equation, overall dynamic response of PMV system can be analyzed by this model. For each several different driving scenario, driving characteristics are shown using simulation.

The in-wheel motor control algorithm consists of three parts. First part is yaw rate controller which generates additional yaw moment to track desired yaw rate for maneuverability and lateral stability. Second part is torque vectoring process, which determines in-wheel motor's torque command considering additional yaw moment, longitudinal wheel slip mitigation and pitchover

mitigation. Third part is state estimator of which estimated signals are fed back to each yaw rate controller and torque vectoring process. More detailed explanations are presented at chapter 3.

Simulation results to verify controller performance is shown using Matlab/Simulink package under various driving conditions at chapter 4. Vehicle test results are also shown under various driving conditions to demonstrate the designed in wheel motor controller's performance to improve cornering maneuverability, lateral stability, and maintain adequate driving force during acceleration at chapter 5.

Chapter 2

Modeling of personal mobility vehicle

To understand basic dynamic characteristics, PMV modeling is needed to be used in simulation level as a plant which is control object. PMV model consists of tire driving mechanism, tire model, wheel dynamics, and body dynamics. Dynamic modeling is based on Newton-Euler equation and each model component's main parameter is adopted.

2.1 Driving mechanism

For longitudinal driving control, right and left handlebar is pressed by rider's hand at each driving situation. To maintain driving force in driving direction, right handlebar is pressed to generate front two in-wheel motor's torque in positive direction. For braking, left handlebar is pressed to generate front two in-wheel motor's torque in negative direction, which results in reducing driving force.

For lateral steering, rider can control roll bar to steer front two wheels. If rider leans roll bar in left side, front two wheels is steered in left side, which results in PMV's left cornering. On the other hand, if rider leans roll bar in right side, PMV is steered in right direction, which results in right cornering.

The overall driving characteristic is similar with bicycle or motor cycle. When rider turns along the corner, for example, rider's body should be tilted to cornering direction to overcome centrifugal force. Tilting rider's body, pedal for acceleration or brake is controlled by rider's hand to maintain proper longitudinal speed. Steering is completed through leaning roll bar with same direction of body tilting, which corresponds with cornering direction.

2.2 Brush tire model

The brush tire model [Pacejka 05] figure is shown as Figure 2.1.

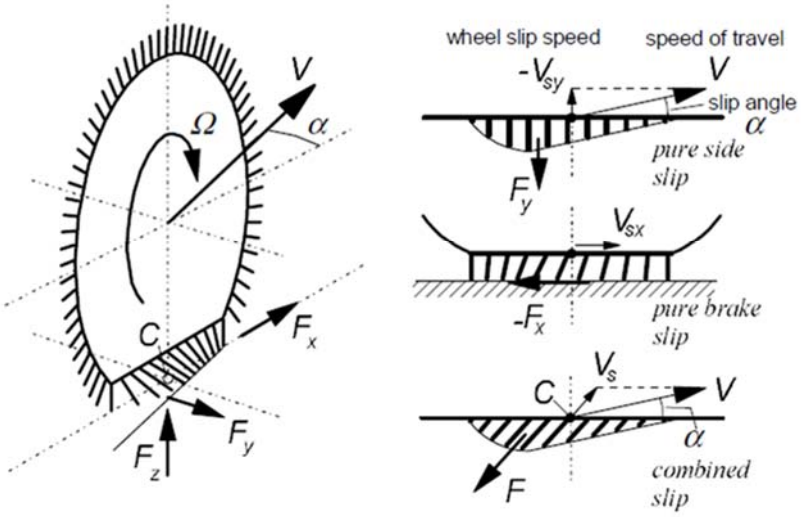

Figure 2.1 Brush tire model

The brush tire model is a mathematical representation of tire longitudinal and lateral force, which is the fundamental driving force of vehicle dynamics. Brush tire model assumes that tire material is isotropic, and that tire force is proportional to tire vertical force. For PMV tire model, combined longitudinal and lateral model is adopted.

Tire forces are function of slip quantities [Rajamani 11], which are also function of tire specific parameters. Longitudinal and lateral slip quantities are defined as following (2.1), (2.2), and (2.3).

$$\kappa = \frac{r \cdot \Omega - V}{V} \tag{2.1}$$

$$\alpha_{fr} = \delta_{fr} - \tan^{-1}\left(\frac{V_y + l_f \cdot \gamma}{V_x + t_w \cdot \gamma}\right) \tag{2.2}$$

$$\alpha_{fl} = \delta_{fl} - \tan^{-1}\left(\frac{V_y + l_f \cdot \gamma}{V_x - t_w \cdot \gamma}\right) \tag{2.3}$$

These slip quantities are called practical slip quantities. Theoretical slip quantities are also defined using those practical slip quantities.

$$\sigma_x = \frac{\kappa}{1+\kappa} \tag{2.4}$$

$$\sigma_y = \frac{\tan\alpha}{1+\kappa} \tag{2.5}$$

$$\sigma = \sqrt{{\sigma_x}^2 + {\sigma_y}^2} \tag{2.6}$$

These theoretical slip quantities are integrated with isotropic model parameter to calculate tire contact force as following (2.7), (2.8) and (2.9).

$$\sigma_{sl} = \frac{1}{\theta} = \frac{3\mu \cdot F_z}{2c_p \cdot a^2} \tag{2.7}$$

$$\begin{aligned} &F = \mu F_z \left\{ 3\theta\sigma - 3\theta^2\sigma^2 + \theta^3\sigma^3 \right\} \ \ for \ \ \sigma \le \sigma_{sl} \\ &F = \mu F_z \ \ \ for \ \ \sigma > \sigma_{sl} \end{aligned} \tag{2.8}$$

$$F_x = F \cdot \frac{\sigma_x}{\sigma},\ F_y = F \cdot \frac{\sigma_y}{\sigma} \tag{2.9}$$

Longitudinal tire force directly contributes to longitudinal acceleration of vehicle, and lateral force contributes to cornering.

2.3 Wheel dynamics

Wheel acceleration is affected by longitudinal tire force which is determined by brush tire model equation. Wheel dynamics [Rajamani 11] is shown as Figure 2.2.

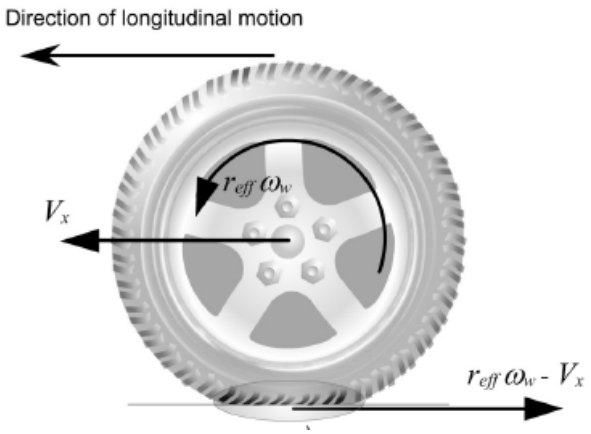

Figure 2.2 Wheel dynamics

Wheel acceleration is calculated by following (2.10)

$$\dot{\Omega} = \frac{T - r \cdot F_x}{I_w} \tag{2.10}$$

2.4 Body dynamics

The overall system is combined with rider body and PMV body. Using tire external forces, Newton-Euler equation should be applied to each rider's body and PMV body, respectively. However, for simplicity of calculation, this study assumed that the rider and PMV system is a single rigid body because rider's mass accounts for most portion of total system.

The rider's tilting angle is determined by lateral acceleration and gravity under the assumption of lateral equilibrium to overcome centrifugal force as Figure 2.3.

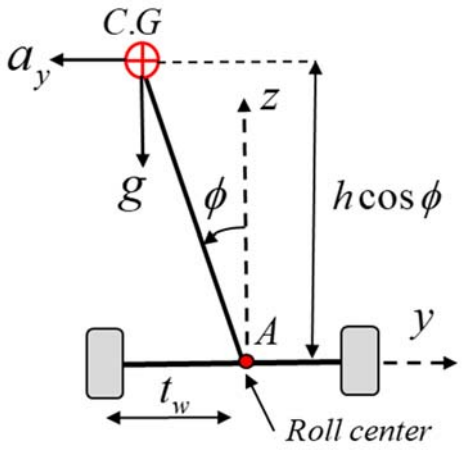

Figure 2.3 Front view of PMV system

The detailed value of tilting angle is shown as following (2.11).

$$m \cdot a_y \cdot h\cos\phi + m \cdot g \cdot h\sin\phi = 0$$

$$\rightarrow \phi = -\tan^{-1}\left(\frac{a_y}{g}\right) \tag{2.11}$$

The tire vertical forces are presented as function of lateral acceleration, longitudinal acceleration, body tilting angle, and gravity as equation (2.12), (2.13) and (2.14)

$$F_{z\_FR} = \frac{mg}{4} + \frac{ma_y h\cos\phi}{2t_w} + \frac{mgh\sin\phi}{2t_w} - \frac{ma_x h\cos\phi}{2(l_f + l_r)} \tag{2.12}$$

$$F_{z\_FL} = \frac{mg}{4} - \frac{ma_y h\cos\phi}{2t_w} - \frac{mgh\sin\phi}{2t_w} - \frac{ma_x h\cos\phi}{2(l_f + l_r)} \tag{2.13}$$

$$F_{z\_R} = \frac{mg}{2} + \frac{ma_x h\cos\phi}{(l_f + l_r)} \tag{2.14}$$

Based on tire external forces and steer angle, Newton-Euler equation is applied to system. The main axes which are fixed with body frame are 3 axes, of which directions are longitudinal, lateral and yaw direction. The overall contour of PMV system and 3 main axes are shown as Figure 2.4.

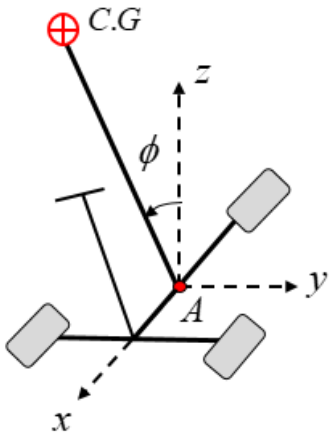

Figure 2.4 Three dimensional view of PMV

Newton-Euler equations for x, y axis are expressed as following (2.15), (2.16).

$$\sum_{i=1}^{3}(F_{xi}\cdot\cos\delta_i - F_{yi}\cdot\sin\delta_i) = m\cdot a_x \tag{2.15}$$

$$\sum_{i=1}^{3}(F_{xi}\cdot\sin\delta_i + F_{yi}\cdot\cos\delta_i) = m\cdot a_y \tag{2.16}$$

Yaw moment equation for z axis is expressed as follow (2.17)

$$\begin{aligned} &l_f\cdot(F_{x1}\cdot\sin\delta_1 + F_{y1}\cdot\cos\delta_1 + F_{x3}\cdot\sin\delta_3 + F_{y3}\cdot\cos\delta_3) \\ &-l_r\cdot F_{y2} \\ &+t_w(F_{x1}\cdot\cos\delta_1 - F_{y1}\cdot\sin\delta_1 - F_{x3}\cdot\cos\delta_3 + F_{y3}\cdot\sin\delta_3) = I_z\cdot\dot{\gamma} \end{aligned} \tag{2.17}$$

Although 3D body rotation effects such as Coriolis terms are neglected, this simplified plane dynamics model can represent general dynamic characteristics at specific driving scenario. For example, tire saturation percentage as vehicle turns with acceleration can be calculated by this simplified PMV model using Matlab/Simulink package to analyze lateral stability of system. More specific examples of this PMV model's dynamic characteristics are shown at chapter 4 in simulation level.

Chapter 3

In-wheel motor control algorithm

3.1 Overall control scheme

Control algorithm determines in-wheel motor's torque command considering yaw rate tracking for maneuverability and stability, longitudinal wheel slip mitigation, and pichover mitigation. Yaw rate controller decides additional yaw moment to track desired yaw rate which is designed using two dimensional bicycle model response. Torque vectoring distributes left and right motor torque command to generate yaw moment. These in-wheel motor torque command is

once saturated through slip mitigation and pitchover mitigation logic.

Control algorithm adopts model based feedback control law which needs system's states. For accurate control input decision, several state estimators are also designed. Overall block diagram of control algorithm is shown as Figure 3.1, which consist of yaw rate controller, torque vectoring, state estimator and plant.

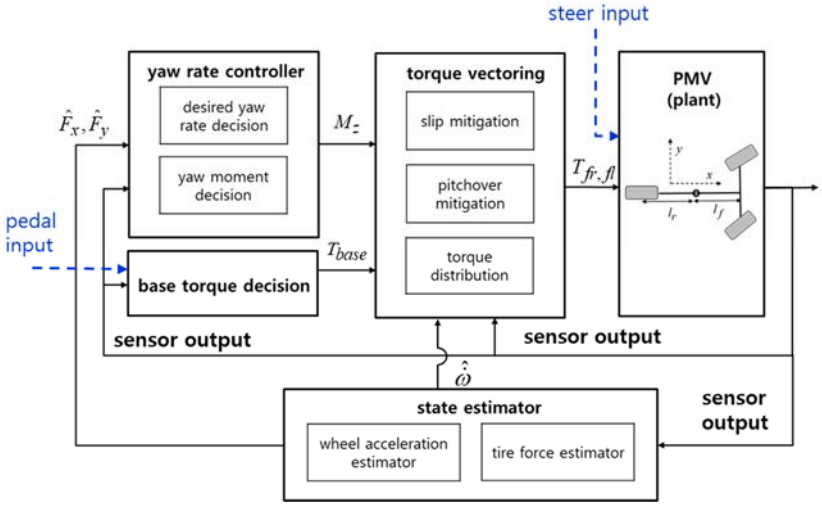

Figure 3.1 Block diagram of PMV control algorithm

3.2 Yaw rate controller

For many vehicle control system, yaw rate controller is an important component of ESC for lateral stability control, maneuverability control. For example, Mokhiamar et al [Imech 02] designed desired yaw rate based on 2nd order bicycle yaw rate response transfer fucntion as a target yaw rate for lateral stability control [Mokhiamar 02]. For this study, two dimensional yaw rate

response model is adopted as a desired yaw rate to be tracked by controller like many kinds of other conventional works [Mokhiamar 02, Hosaka 04, Ando 10]. However, one distinct identity for this study is that understeer gradient which is a parameter of desired yaw rate is designed as a function of longitudinal speed to consider different system dynamic characteristics along longitudinal speed.

Overall scheme of yaw rate controller is presented as Figure 3.2. Each component of yaw rate controller is explained based on mathematical background.

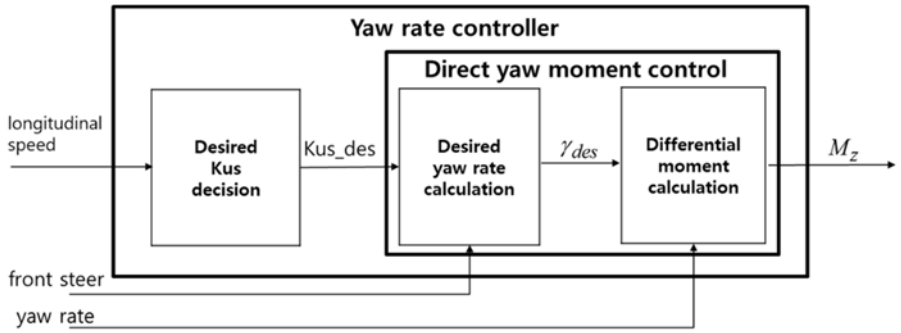

Figure 3.2 Overall scheme of yaw rate controller

Desired understeer gradient which is a fundamental indicator of vehicle system performance should be designed to be used as a parameter of desired yaw rate. Two dimensional bicycle yaw rate response model is shown as following (3.1), which is combined with understeer gradient, longitudinal speed, and front steer angle.

$$\gamma = \frac{V_x}{l_f + l_r + K_{base} \cdot {V_x}^2} \cdot \delta \tag{3.1}$$

For appropriate desired yaw rate, understeer gradient should be designed considering tire saturation region to prevent lateral instability. Tire saturation region is shown as following Figure 3.3.

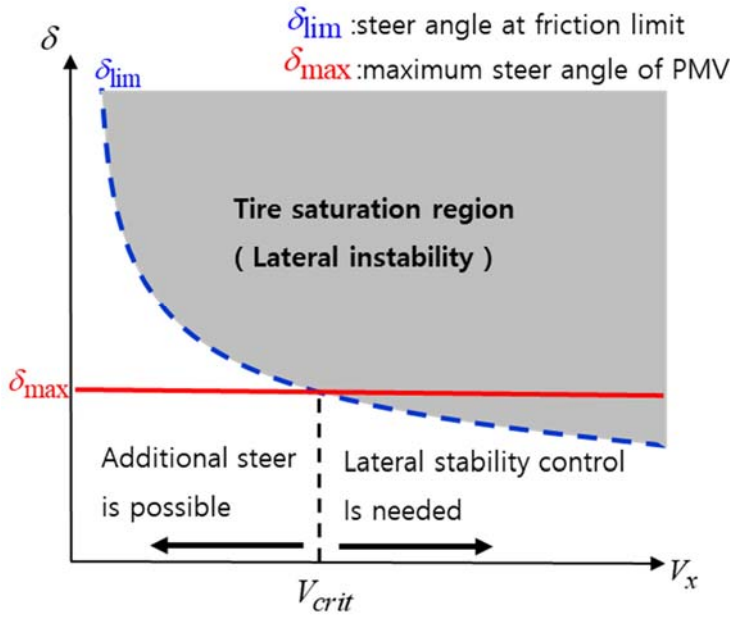

Figure 3.3 Tire saturation region along vehicle states

For lower speed than critical speed, additional front steering can be applied to vehicle, which means that additional yaw rate can be generated because the margin to friction limit exists. However, at higher speed than critical speed, lateral instability can occur when trying front steering because steer angle at

friction limit is lower than vehicle's maximum steer angle. To avoid such lateral instability, lateral acceleration should be upper bounded under friction limit value. Based on such criterion, steer angle at friction limit and critical speed is calculated before designing desired understeer gradient.

$$\frac{V_x}{l_f + l_r + K_{base} \cdot V_x^2} \cdot \delta_{\lim} = \frac{\mu \cdot g}{V_x},$$

$$\delta_{\lim} = \frac{\mu \cdot g}{V_x^2} \cdot (l_f + l_r + K_{base} \cdot V_x^2) \tag{3.2}$$

$$\begin{aligned} \delta_{\lim} &= \frac{\mu \cdot g}{V_x^2} \cdot (l_f + l_r + K_{base} \cdot V_x^2) \\ &= \delta_{\max}, \end{aligned}$$

$$V_x = V_{crit} = \sqrt{\frac{\mu \cdot g \cdot (l_f + l_r)}{\delta_{\max} - \mu \cdot g \cdot K_{base}}} \tag{3.3}$$

If PMV follows the desired understeer gradient and corresponding yaw rate during maximum front steering, the lateral acceleration should not be higher than that of friction limit. Based on this physical constraint, desired understeer gradient and yaw rate can be designed as follows.

$$\gamma_{des}(\delta_{\max}) = \frac{V_x}{l_f + l_r + K_{us\_des} \cdot {V_x}^2} \cdot \delta_{\max}$$
$$= \frac{\mu \cdot g}{V_x},$$

$$K_{us\_des} = -\frac{(l_f + l_r)}{{V_x}^2} + \frac{\delta_{\max}}{\mu \cdot g} \tag{3.4}$$

$$\gamma_{des} = \frac{V_x}{l_f + l_r + K_{us\_des} \cdot {V_x}^2} \cdot \delta \tag{3.5}$$

At speed below critical speed, base model's understeer gradient is higher than desired understeer gradient due to the fact that maximum steer is lower than steer angle at friction limit by Fig 3.3, (3.2) and (3.4). However, at speed higher than critical speed, desired understeer gradient is higher than that of base model due to lower value of steer angle at friction limit compared with maximum steer angle of PMV. By combining this understeer gradient's comparison and (3.1), it can be induced that desired yaw rate at speed lower than critical speed is greater than that of base model, and for the other case, desired yaw rate is lower than that of base model. In other words, if PMV tracks desired yaw rate, maneuverability is increased due to higher yaw rate compared to that of base model at low speed, and lateral acceleration is saturated below the friction limit at high speed due to lower yaw rate compared to that of base model. This characteristic is shown as Figure 3.4.

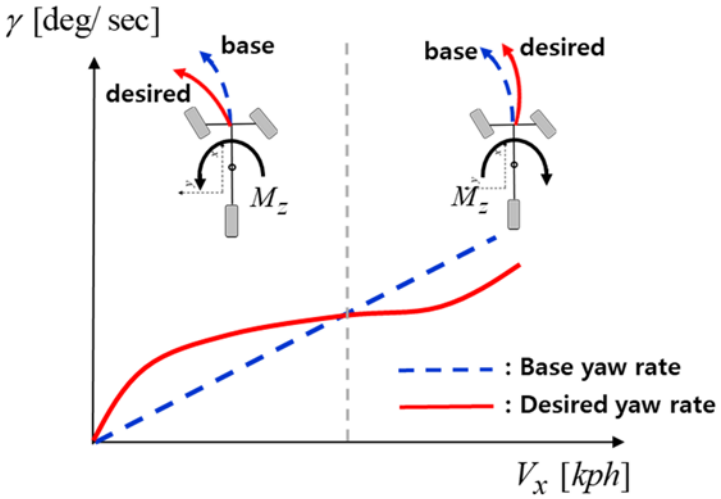

Figure 3.4 Yaw rate and yaw moment direction along vehicle speed

To track desired yaw rate, sliding mode control method is adopted [Kang 11]. Tracking error, which is same as sliding surface, is designed as equation (3.6).

$$s = e = \gamma - \gamma_{des} \tag{3.6}$$

To design controller, Lyapunov function V should be determined to apply lyapunov stability criterion as following (3.7).

$$V = \frac{1}{2}s^2 \tag{3.7}$$

Lyapunov stability criterion is presented as following equation (3.8), which is

necessary and sufficient condition for the convergence of system's state to sliding surface.

$$\begin{aligned} &\dot{V} = s \cdot \dot{s} = -K \cdot |s| < 0, \\ &\dot{s} = -K \cdot sign(s) \end{aligned} \tag{3.8}$$

The above Lyapunov stability criterion is combined with yaw moment equation of vehicle, to represent control input in terms of system's state and sliding surface as following (3.9).

$$\begin{aligned} \dot{s} &= \dot{\gamma} - \dot{\gamma}_{des} \\ &= \frac{M_z}{I_z} + \frac{\hat{F}_{yf} \cdot l_f - \hat{F}_{yr} \cdot l_r}{I_z} - \dot{\gamma}_{des} \\ &= -K \cdot sign(s), \end{aligned}$$

$$M_z = \overbrace{I_z \cdot \dot{\gamma}_{des} - \hat{F}_{yf} \cdot l_f + \hat{F}_{yr} \cdot l_r}^{feedforward} - \overbrace{K \cdot I_z \cdot sign(s)}^{feedback} \tag{3.9}$$

When system's state converges to sliding surface, chattering phenomenon could occur. To avoid such vibration of state near the sliding surface, saturation function is adopted to feedback terms of control input as following (3.10), which is the final representation of yaw rate controller's yaw moment.

$$M_z = I_z \cdot \dot{\gamma}_{des} - \hat{F}_{yf} \cdot l_f + \hat{F}_{yr} \cdot l_r - K \cdot I_z \cdot sat(\frac{\gamma - \gamma_{des}}{\phi}) \tag{3.10}$$

This yaw moment control input signal goes into torque vectoring logic to distribute above yaw moment to each front motor as differential torque.

3.3 Torque vectoring

In torque vectoring logic, three main processes exist, which are yaw moment distribution, wheel slip mitigation, and pitchover mitigation. Each processes are operated in sequential step.

For yaw moment distribution, yaw moment input which is generated in yaw rate controller is distributed at each front left wheel and right wheel motor as following (3.11).

$$\Delta T_{diff} = \frac{r \cdot M_z}{2 \cdot t_w} \tag{3.11}$$

These differential torque is added to each right and left in-wheel motor's base torque as following (3.12).

$$T_{com\_l} = T_{base} - \Delta T_{diff}$$

$$T_{com\_r} = T_{base} + \Delta T_{diff} \tag{3.12}$$

These left, right command torque is then processed by wheel slip mitigation

logic. Wheel slip mitigation logic adds additional torque to each wheel to avoid tire longitudinal saturation considering tire saturation characteristic which is presented as Figure 3.5.

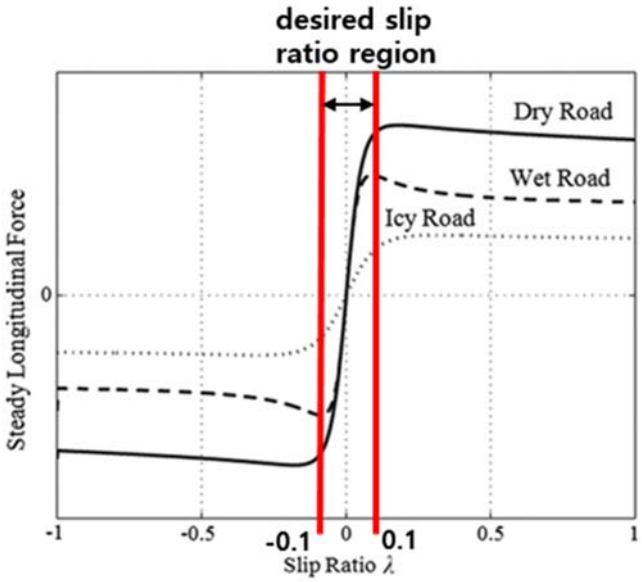

Figure 3.5 Tire longitudinal force along the slip ratio

To avoid tire longitudinal slip, tire slip ratio, which is the ratio of wheel rolling speed to longitudinal speed, should be calculated to determine additional torque as other conventional works [Harifi 08]. However, in PMV system which is used for this study, there is no rear wheel encoder which is needed to know longitudinal speed information. To cope with such hardware situation, wheel acceleration and longitudinal acceleration is used to determine additional torque as follows.

$$T_{com} = T_{base} \pm \Delta T_{diff} + \Delta T_{slip},$$

$$\Delta T_{slip} = -k_p(r \cdot \hat{\dot{\omega}} - a_x) - k_i \int (r \cdot \hat{\dot{\omega}} - a_x)\, dt \quad for\ r \cdot \left|\hat{\dot{\omega}}\right| > |a_x| + \beta \tag{3.13}$$

This additional slip torque is based on PI control of rolling acceleration and longitudinal acceleration. If the rolling acceleration is too larger than longitudinal acceleration, additional torque in counter direction is added to each wheel to prevent over slip of wheel. However, due to lack of speed information, this slip mitigation logic has limitations in use, especially when wheel slip situation occurs at steady state of vehicle. This slip mitigation logic is only meaningful when the vehicle starts to accelerate or brake suddenly.

The base torque is also saturated for avoiding pitchover situation. Pitchcover is defined as a case when the vehicle's front or rear wheel's vertical force becomes zero. To make vehicle not to encounter such wheel lift situation, longitudinal acceleration should be saturated appropriately.

The tire vertical forces for front and rear should be calculated as shown as following (3.14) including pitch angle.

$$F_{z\_r} = \frac{m \cdot g}{2}\cos(p) + \frac{m \cdot h \cdot a_x}{L} - \frac{2 \cdot m \cdot g \cdot h \cdot \sin(p)}{L}$$
$$F_{z\_f} = \frac{m \cdot g}{2}\cos(p) - \frac{m \cdot h \cdot a_x}{L} + \frac{2 \cdot m \cdot g \cdot h \cdot \sin(p)}{L} \tag{3.14}$$

When equation (3.14) becomes zero, each case is front or rear wheel lift situation. Acceleration at each wheel lift can be calculated by solving (3.14) to

be zero as following (3.15)

$$a_{x\_upp} = \frac{L \cdot g}{2h}\cos(p) + 2g \cdot \sin(p)$$
$$a_{x\_low} = -\frac{L \cdot g}{2h}\cos(p) + 2g \cdot \sin(p) \quad (3.15)$$

Longitudinal acceleration should be saturated between those two boundary values. Upper and lower bound of base torque for saturation is finally calculated by (3.16).

$$T_{base\_sat\_upp} = \frac{m \cdot r}{2}(a_{x\_upp} - g \cdot \sin(p)),$$
$$T_{base\_sat\_low} = \frac{m \cdot r}{2}(a_{x\_low} - g \cdot \sin(p)) \quad (3.16)$$

When base torque is determined by rider's acceleration or brake pedal input, base torque is saturated based on those two saturation torque value. By saturating base torque, longitudinal acceleration of vehicle cannot exceed limitation values of (3.15).

3.4 State estimator

State estimation is needed to determine yaw moment at yaw rate controller. Especially lateral forces should be estimated to be used at yaw rate controller.

Lateral forces are estimated based on dynamics equation as following (3.17).

$$\hat{F}_{yf} \cdot l_f - \hat{F}_{yr} \cdot l_r + M_{z\_pre} \approx 0$$

$$\hat{F}_{yf} + \hat{F}_{yr} = m \cdot a_y \tag{3.17}$$

By solving upper two simultaneous equations, lateral force of each front and rear tire can be estimated based on assumption of yaw moment equilibrium. In (3.17), present yaw moment is used, and its value can be calculated by estimated longitudinal forces which is also estimated through state estimator.

To estimate longitudinal tire forces, wheel angular acceleration should be estimated. Wheel angular acceleration is estimated by kalman filter, which uses process update and measurement update equations [Faragher 12]. The state equation of wheel angular acceleration is obtained by the Taylor formula as following (3.18).

$$\omega_i(t+\Delta T) = \omega_i(t) + \Delta T \cdot \dot{\omega}_i(t) + \frac{\Delta T^2}{2}\ddot{\omega}_i(t) + d_1$$

$$\dot{\omega}_i(t+\Delta T) = \dot{\omega}_i(t) + \Delta T \cdot \ddot{\omega}_i(t) + d_2$$

$$\ddot{\omega}_i(t+\Delta T) = \ddot{\omega}_i(t) + d_3 \tag{3.18}$$

Measurement equation is expressed as following (3.19).

$$y(t) = [1 \quad 0 \quad 0] \cdot [\omega_i(t) \quad \dot{\omega}_i(t) \quad \ddot{\omega}_i(t)]^T \tag{3.19}$$

The state equation for kalman filter to estimate wheel angular acceleration is presented as following (3.20) which is based on (3.18) and (3.19).

$$x(k+1) = \overbrace{\begin{bmatrix} 1 & \Delta T & \Delta T^2/2 \\ 0 & 1 & \Delta T \\ 0 & 0 & 1 \end{bmatrix}}^{A_{esti}} \cdot \begin{bmatrix} \omega_i(k) \\ \dot{\omega}_i(k) \\ \ddot{\omega}_i(k) \end{bmatrix} + \overbrace{\begin{bmatrix} 1 & 0 & 0 \\ 0 & 1 & 0 \\ 0 & 0 & 1 \end{bmatrix}}^{G_{esti}} \cdot \begin{bmatrix} d_1 \\ d_2 \\ d_3 \end{bmatrix}$$

$$y(k) = \overbrace{[1 \quad 0 \quad 0]}^{H_{esti}} \cdot x(k) + v(k) \tag{3.20}$$

Based on these process and measurement equations, state estimation is finally represented as following (3.21).

$$x(k \mid k) = A_{esti} \cdot \hat{x}(k-1 \mid k-1) + L(k) \cdot \{ y(k) - H_{esti} \cdot A_{esti} \cdot \hat{x}(k-1 \mid k-1) \} \tag{3.21}$$

Second component of estimated states is the wheel angular acceleration, which is the target estimated state. This estimated wheel angular acceleration is used at torque vectoring process to determine additional torque to avoid wheel

slip. Using this wheel angular acceleration, tire longitudinal forces are estimated based on wheel dynamics as shown as (3.22).

$$\hat{F}_{x\_i}(k) = \frac{1}{r} \cdot \{T_i(k) - \frac{1}{I_w} \cdot \hat{\dot{\omega}}_i(k \mid k)\} \tag{3.22}$$

Using this longitudinal tire forces, present yaw moment due to longitudinal tire forces can be calculated to be used at (3.17) as following (3.23).

$$M_{z\_pre} = \hat{F}_{x\_r} \cdot t_w - \hat{F}_{x\_l} \cdot t_w \tag{3.23}$$

All the states which are estimated such as longitudinal, lateral tire forces and wheel angular acceleration are fed back to yaw rate controller and torque vectoring processes as shown at Figure 3.1.

Chapter 4

Simulation results

4.1 Base model's dynamic characteristics

Base model's dynamic characteristics are important indicators in that they can show the basic performances of vehicle. By analyzing basic performances of vehicle based on specific driving situations, the main objective of controller design can be presented to overcome the drawbacks of vehicle safety and maneuverability. Especially, by using Matlab/Simulink package, dynamic performances can be presented in simulation level with designed vehicle models.

The overall parameters which are used in simulation level are shown as Figure 4.1. All the parameter's values are almost same with those of real vehicle system which is used for actual vehicle tests.

parameter	unit	parameter	unit
$2t_w$	$0.49\ m$	x axis-moment of inertia	$36.86\ kg \cdot m^2$
$L = L_f + L_r$	$0.89\ m$	y axis-moment of inertia	$38.01\ kg \cdot m^2$
vehicle mass	$25\ kg$	z axis-moment of inertia	$2.69\ kg \cdot m^2$
rider's mass	$76\ kg$	front wheel radius	$5\ in$
height of C.G	$0.6\ m$	rear wheel radius	$4\ in$
total mass	$101 kg$	friction coefficient	$0.6 \sim 1$
tire cornering stiffness	$3050\ N\ /\ rad$	Contact patch	$0.0254\ m$

Figure 4.1 Vehicle parameters for simulation application

Base model's cornering performances at steady state with different longitudinal speeds are main indicators of characteristics of turning motion of vehicle [Velenis 10]. Lateral acceleration, yaw rate and turning radius are major performance index of vehicle's turning motion. Analyzing these factors, the overall motion characteristics related to lateral stability and turning maneuverability can be understood, which is directly connected to the way of controller design. Maximum possible front steer cornering until friction limit at steady state along different longitudinal speed scenario is used as simulation situation. The simulation results are presented as following Figure 4.2.

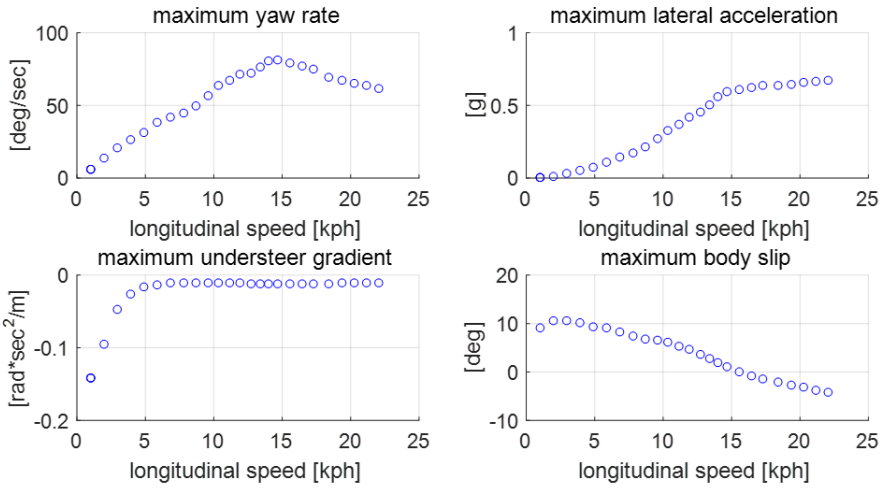

Figure 4.2 Simulation results of maximum possible front steer cornering at steady state along longitudinal speed

As vehicle longitudinal speed increases, the lateral acceleration saturates under 0.6g cause the friction coefficient is about 0.6. Yaw rate of vehicle increases linearly until 15kph, and decreases after that speed. It can be induced that steering angle at friction limit is lower than maximum steer angle of PMV after 15kph which is also shown at Figure3.3. That is the reason why maximum yaw rate should be decreased after 15kph to avoid lateral tire saturation. Resultantly, front steer angle should also be decreased below maximum front steer angle of PMV to lower yaw rate.

The vehicle's overall performance shows that PMV's understeer gradient is negative, which imply oversteer characteristics. This oversteer vehicle's body slip angle diverges as longitudinal speed increases. The reason why oversteer vehicle's body slip angle diverges along the speed is that the rear wheel's slip

angle is much bigger than that of front wheel. As the gap between rear and front wheel's slip angle increases, the body slip also increases. If the body slip angle becomes bigger that specific value, rear wheel encounters lateral saturation, which means lateral instability.

To understand more specifically the oversteer characteristics of vehicle, sineweave simulation [Chung 06] is conducted as following Figure 4.3.

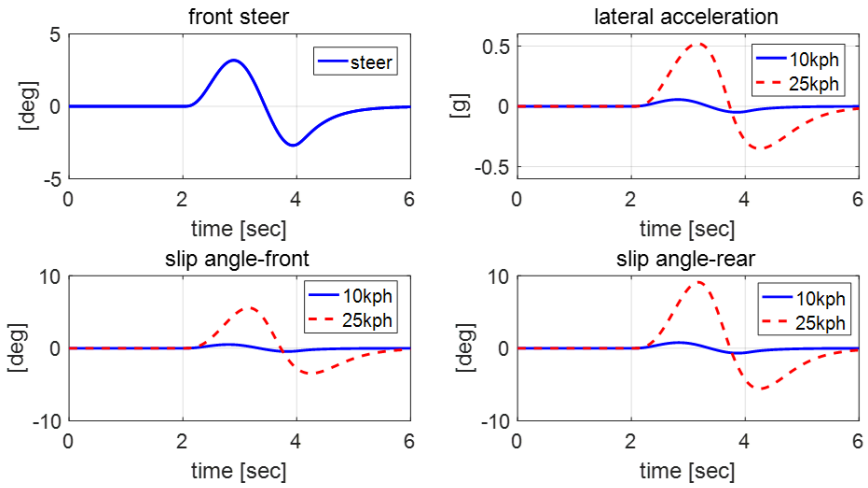

Figure 4.3 Sineweave test results for 10kph, 25kph in simulation level

As shown above figure, the gap between front and rear wheel's slip angle becomes larger as longitudinal speed increases from 10kph to 25kph. As the gap becomes larger until friction limit value, the rear wheel goes through lateral tire saturation. In that case, yaw rate and body slip angle diverges, which is significantly dangerous situation for rider. For lateral stability, lateral acceleration and yaw rate should be controlled to avoid such tire lateral

saturation.

From the above two figures, the main objective of PMV controller is designed considering longitudinal speed. At low speed, maximum yaw rate can increase linearly because the maximum steer angle is much lower than steer angle at friction limit. It means that under 15kph, maximum front steer angle can be given to PMV without losing lateral stability. Resultantly, cornering radius is main issue of controller at this speed region, rather than lateral stability. On the other hand, after 15kph, yaw rate and lateral acceleration should be decreased under friction limit values to maintain lateral stability. More specific explanations of controller's objective is already represented in chapter 3.

Controller performance results are analyzed in next section in simulation level.

4.2 Controller performance verification

In simulation level using Matlab/Simulink package, the yaw rate controller's performance is verified at different longitudinal speed region. At low speed level, desired yaw rate is larger than that of base model, the yaw moment is generated in positive turning direction, which reduces the radius of curvature resultantly. Overall dynamic performance at low speed with constant steering step input scenario is shown as Figure 4.4.

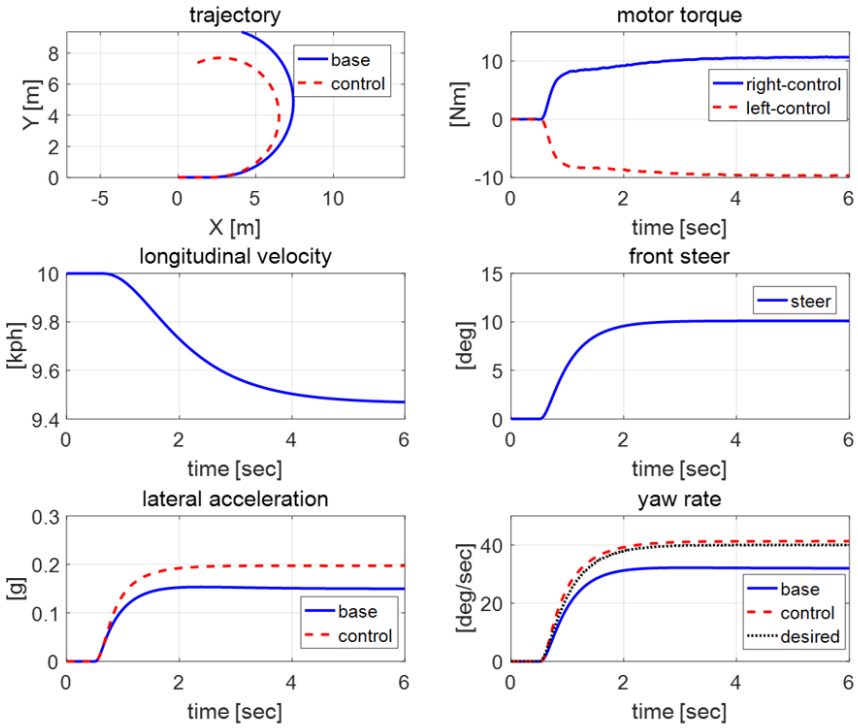

Figure 4.4 Simulation results at 10kph with step front steer

Lateral acceleration and yaw rate are increased as following the desired yaw rate by controller. As a result, the turning radius of trajectory is significantly reduced as shown above figure. The differential torque is commanded at each front in-wheel motor. When the vehicle turns left, the right torque is in positive direction because the yaw moment is in counterclockwise direction. Vehicle's longitudinal speed doesn't change for each base and controlled model cause the summation of differential torque is zero, which means the total wheel torque's summation is same with that of each wheel's base torque. By this simulation result, it can be induced that the cornering maneuverability increases by yaw

rate controller at relatively low speed region.

In other case, for relatively high speed, tire saturation can occur which result in lateral side slip. To prevent such lateral instability, controller should saturate lateral acceleration under friction limit value. The overall dynamic performance for each base model and controlled model is shown as Figure 4.5.

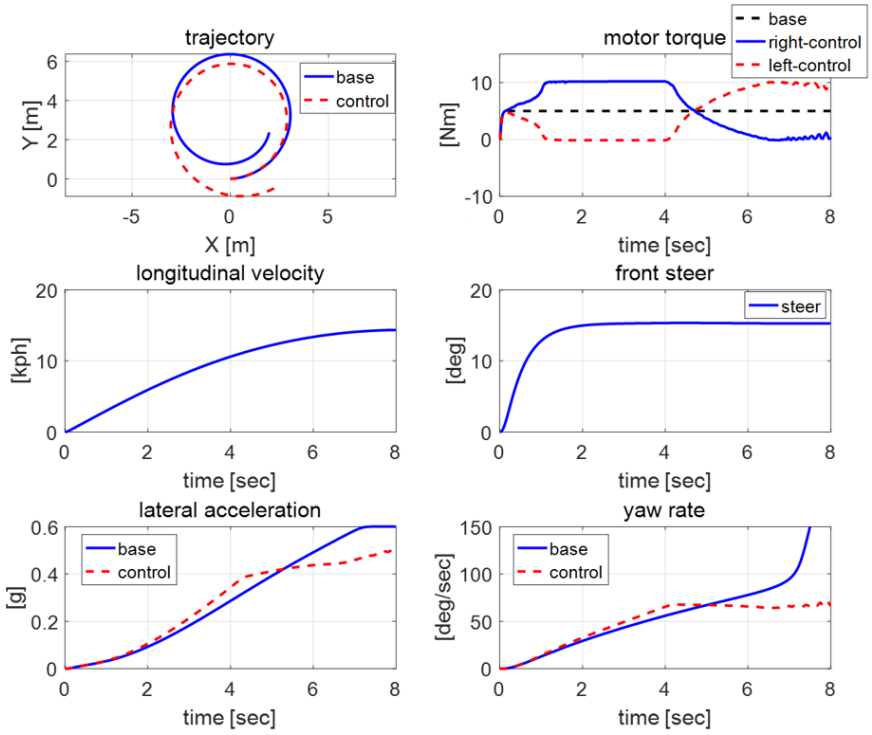

Figure 4.5 Simulation results with step front steer during acceleration

In base model's case, yaw rate increases approximately in linear until 7 second. After that, yaw rate begins to diverge as lateral acceleration reaches 0.6g, which is value of friction limit. This implies that vehicle encounters lateral side slip

due to tire saturation. To make vehicle drive in laterally stable region, lateral acceleration should be reduced by yaw rate controller as shown as Figure 4.5. By yaw rate controller, differential torque is determined to generate clockwise yaw moment at high speed, which results in reduced lateral acceleration. Actually, right motor torque is lower than that of left motor after 5 second to cope with relatively high speed region's problem.

More information of tire saturation is analyzed as Figure 4.6 which is same simulation scenario with Figure 4.5 to understand tire dynamic response [Outfroukh 11].

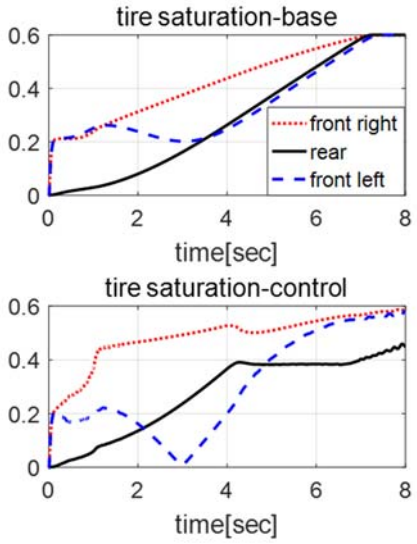

Figure 4.6 Tire saturation results with same scenario of Figure 4.5

For the base model case, rear tire's saturation, which is the ratio of vertical tire force to planar tire force, increases much fast that the other wheels. When rear

wheel's saturation encounters 0.6, which is friction coefficient, rear tire begins to lateral slip and resultantly, the vehicle loses stability. However by controlling the yaw rate of vehicle generating differential torque, rear tire's saturation significantly reduces as Figure 4.6. By preventing lateral slip due to oversteer, yaw rate doesn't diverge without losing lateral stability as shown as Figure 4.5 and 4.6.

Other controller's performance's verifications such as slip mitigation and pitchover mitigation are skipped in simulation level. These controller's performance is shown in vehicle test results in chapter 5. Based on numerical simulation with specific driving scenarios, yaw rate controller's performances are analyzed. The overall objective of controller is satisfied through determining yaw moment as a function of longitudinal speed which are shown as above simulation results.

Chapter 5

Vehicle test results

5.1 Yaw rate controller verification

Yaw rate controller's performance for relatively low velocity can be shown by openloop test. For openloop test, roll bar is fixed to maintain constant front steer angle. In that case, by using controller, yaw rate is increased which means the decrease of radius of curvature at low speed. One example of such openloop test for yaw rate controller's verification is shown as Figure 5.1. .

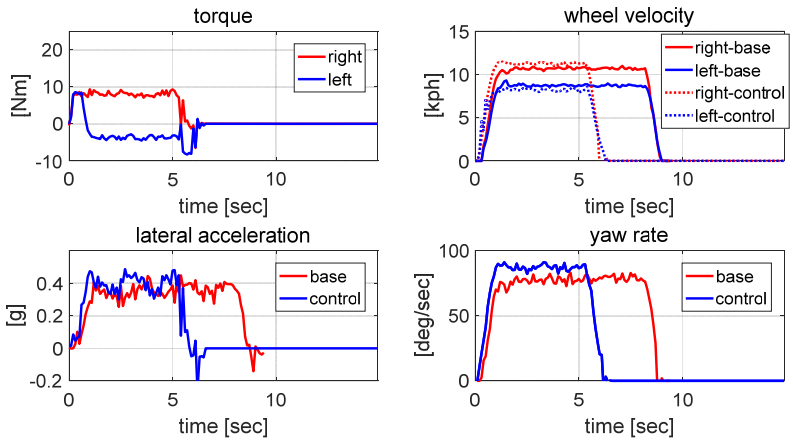

Figure 5.1 Cornering test at constant 26deg front steer at 10kph

In Figure 5.1, by yaw rate controller, controlled model's yaw rate and lateral acceleration is increased cause of differential wheel torque.

For each different longitudinal speed and steer angle, openloop tests like Figure 5.1 are complemented. Each base and controlled case is compared using yaw rate, lateral acceleration and radius of curvature. Yaw rate and lateral acceleration is measured through 9-DOF IMU and radius of curvature is calculated in off-line. The result at 12deg of front steer angle for dry asphalt condition is shown as Figure 5.2.

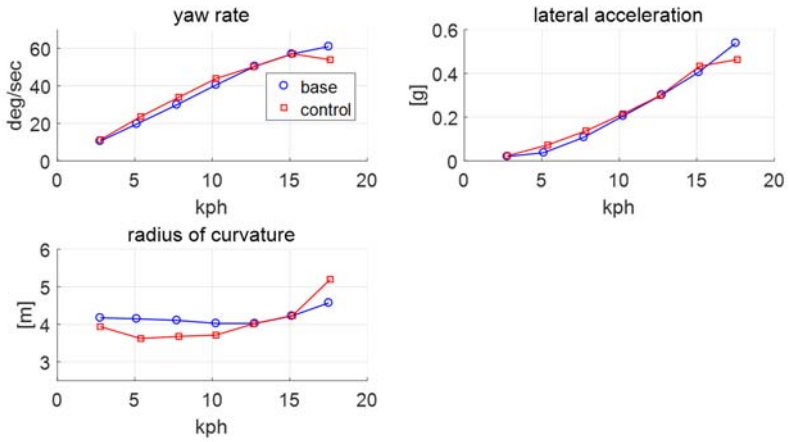

Figure 5.2 Test results at 12deg front steer in dry asphalt along longitudinal speed

As shonwn as above figure, yaw rate and lateral acceleration is increased in low speed regioni under 15kph. As a result, radius of curvature is decreased about 0.7m at 5kph. However, at high speed region, cause of the direcion of yaw moment, controlled model's yaw rate and lateral acceleration is decreased compared with base model.

For low velocity with different road condition of which friction coefficient is about 0.6 with 15deg constant steer angle, openloop test result is shown as Figure 5.3.

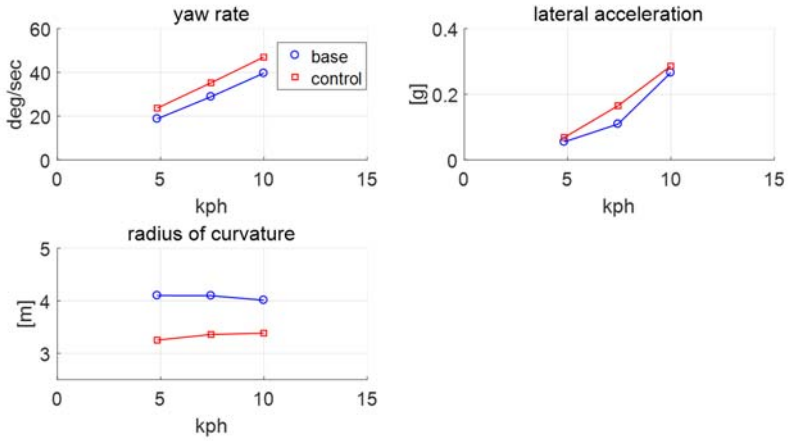

Figure 5.3 Test results at 18deg front steer in wet road along longitudinal speed

For relatively low velocity, the radius of curvature is decreased about 1m. Although the decrease of radius of curvature at Figure 5.2 and 5.3 is different each other cause of different steer angle and friction coefficient, the radius of curvature is significantly decreased about 0.7~1 m, which means the improvement of cornering maneuverability.

Lateral stability improvement at high speed region is verified through same type openloop test. Front steer angle is maximum to make vehicle encounter tire saturation with wet road. The result at relatively wet road with maximum steer angle about 26deg is shown as Figure 5.4.

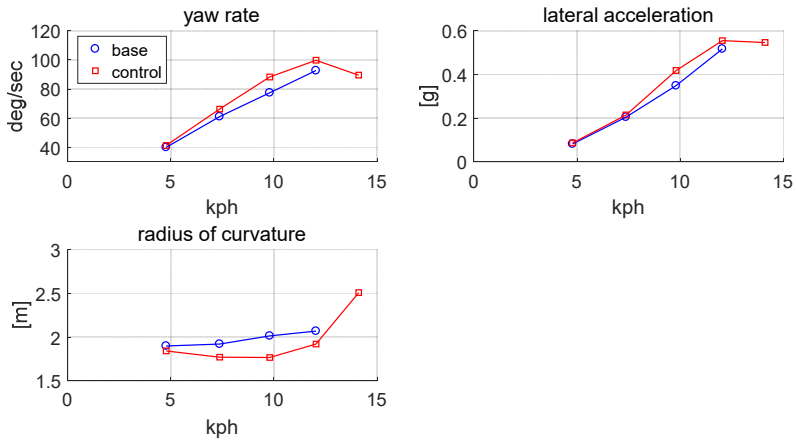

Figure 5.4 Test results at 26deg front steer in wet road along longitudinal speed

Around 15kph, base model's lateral acceleration encounters 0.6g, which is the value of friction limit. At this case, tire lateral saturation occurs and lateral stability is not maintained. Resultantly, vehicle loses controllability under oversteer tire saturation situation, which results in the divergence of yaw rate as Figure 4.5. That is the reason why data at 15kph is missed in Figure 5.4, which implies the vehicle cannot drive in steady state. However, by controlling the vehicle, vehicle's lateral acceleration is saturated under 0.6g as shown as above graphs. Rear tire's saturation is avoided as a result, and the vehicle can drive in steady state around 15kph, which is impossible for base model. By using yaw rate controller, lateral stability is maintained around friction limit situation as shown as above figure.

The overall control performance during acceleration is also analyzed to verify control input in detail as shown as Figure 5.5.

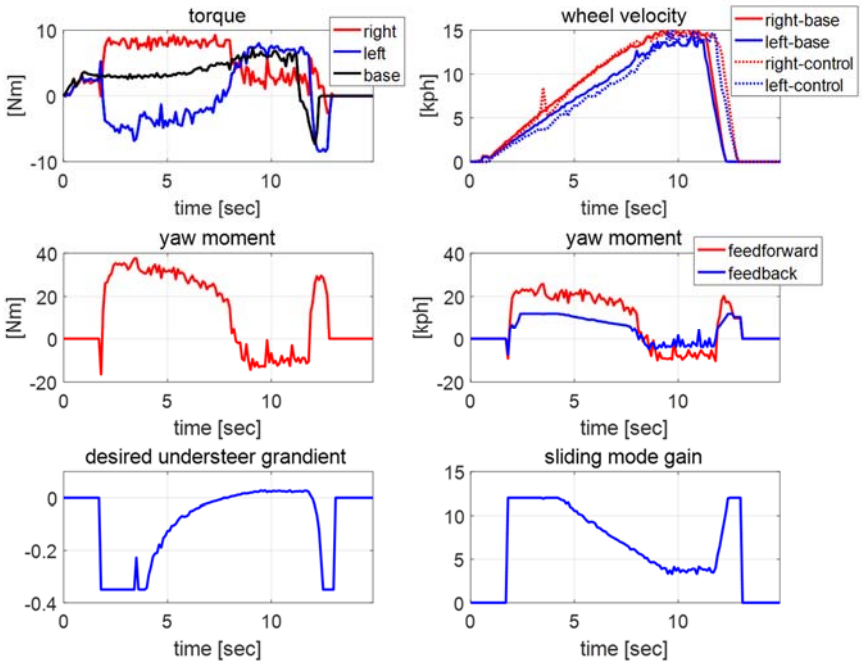

Figure 5.5 Control input and related terms at 26deg front steer in wet road during accleraion and braking

In wheel motor torque of one side is increased or decreased at 8 second with no special divergence. This conversion of relative value of in wheel motor torque can be explained using yaw moment. Yaw moment is positive, which means counterclockwise direction before 8 second. However this direction is changed after that time below zero, which is negative. The instant jumping of yaw moment after 12 second is due to braking. Yaw moment can be separated into feedforward and feedback terms as shown as equation (3.9). For stable convergence of state, feedforward term is bigger than that of feedback.

Another important indicator is that the sliding mode gain is changing along the longitudinal speed. To prevent large chattering effect during state convergence, feedback gain should be tuned for each longitudinal speed as

shown as above figure. Sliding mode gain is decreasing as speed increases to avoid chattering effect.

Analyzing yaw rate controller, it is shown that vehicle's maneuverability at low speed region is improved through decreasing the radius of curvature. Also, lateral stability is maintained reducing lateral acceleration at high speed region avoiding lateral side slip which is from tire saturation.

5.2 Wheel slip mitigation verification

Although maintain wheel slip ratio under 0.1 for all the time is difficult cause of the lack of longitudinal speed information, wheel slip mitigation at acceleration or braking is possible saturating the wheel angular acceleration. The test result is shown as Figure 5.6.

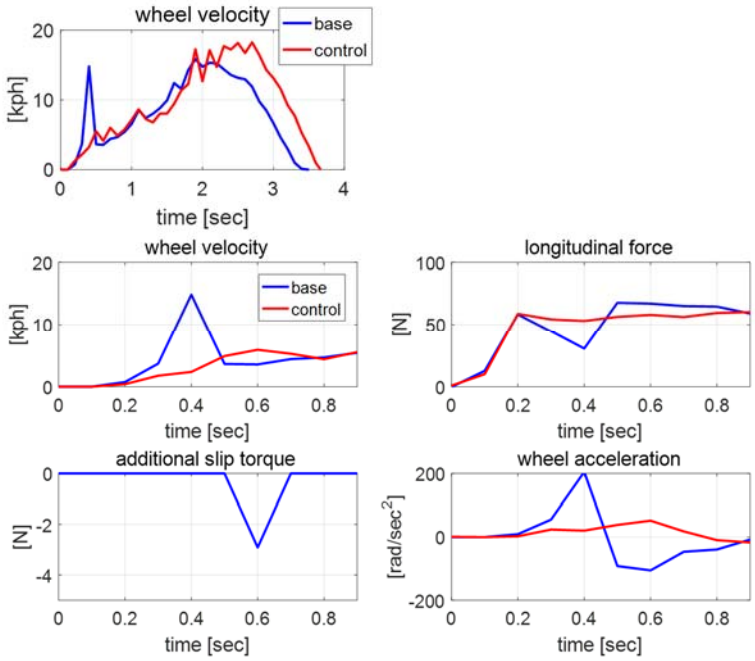

Figure 5.6 Slip related states during linear acceleration

It can be shown that wheel velocity is jumped significantly at 0.4 second cause of longitudinal tire saturation. As a result, tire longitudinal force, which is driving force of vehicle, is reduced suddenly at 0.4 second, which means large wheel slip. By slip mitigation logic, additional slip torque is applied in negative direction to reduce wheel velocity. Resultantly, wheel acceleration and longitudinal force is maintained in adequate level.

By this control logic, driving force reduction during acceleration or braking can be avoided for short time.

5.3 Pitchover mitigation verification

By saturating base torque, longitudinal acceleration can be controlled to avoid longitudinal wheel lift, which is pitchover case. Pitch angle of vehicle is measured through 9-DOF IMU. The test result for braking situation with 15deg grade angle is shown as Figure 5.7.

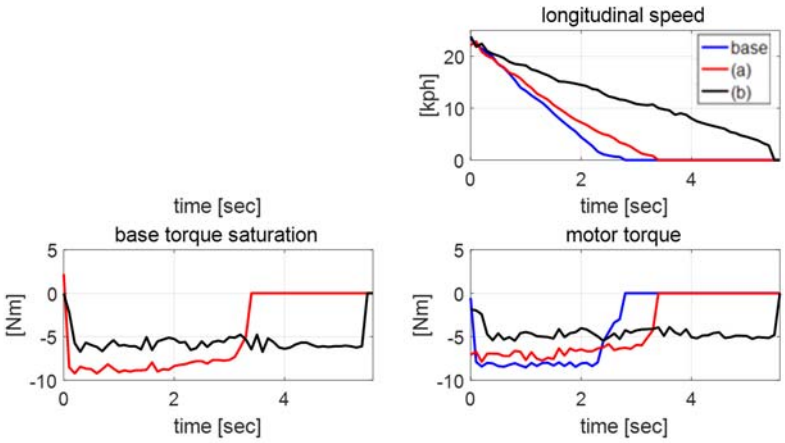

Figure 5.7 Test results of braking with 15deg grade angle

As shown as above figure, base torque is saturated at different level. The slope of decreasing longitudinal speed is determined by saturated base torque, which is acceleration control. By saturating base torque, the acceleration can be changed to avoid pitchover at specific grade angle.

5.4 Wheel acceleration estimator verification

Wheel angular acceleration estimation is important to be used for desired yaw moment decision, longitudinal tire slip mitigation logic. Kalman filter based wheel angular acceleration estimation is verified through linear acceleration test data as Figure 5.8.

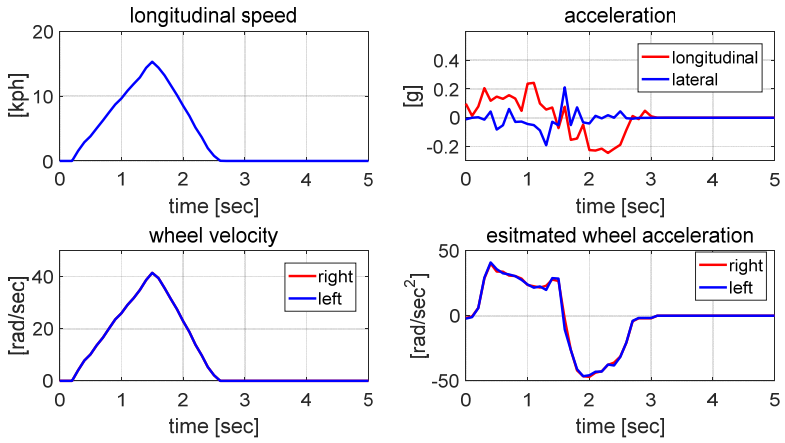

Figure 5.8 Test results of linear acceleration and braking

The slope of wheel velocity, which is mean of wheel acceleration, is shown as above figure. The value is about 35~40 rad per square of second. This value is almost same with that of estimated wheel acceleration as shown as above figure. The kalman filter based wheel angular acceleration estimation logic is verified through linear test results as above graphs.

Chapter 6

Conclusions

In this study, control algorithm for three wheeled PMV is developed and verified through simulation and test results. Yaw rate control algorithm can improve turning manueverability at low speed and also prevent lateral side slip which is due to lateral tire saturation. Wheel slip mitigation logic is embedded to avoid driving force's sudden reduction during accelarion and braking. Longtudianl wheel lift, which is pitchvoer case can be prevented by using pitchvoer mitigation logic which saturates base torque. All the control algorithms are verifired using Matlab/Simuliknk package in simulation level. Finally, embedding these algorithms into test vehicle, various scenario tests are complemented to verify the control algorithm of PMV.

For future works, to cope with the inaccurate friction coefficient, tire force saturaion which is the ratio of vertical force to planar force will be introduced to control logic. Also wheel slip mitigation logic will be improved using other kinds of control theory.

Bibliography

[Hibbard 96] Hibbard, Robin, and Dean Karnopp. "Twenty first century transportation system solutions-A new type of small, relatively tall and narrow active tilting commuter vehicle." *Vehicle system dynamics* 25.5: 321-347, 1996.

[Gohl 06] Gohl, J., et al. "Development of a novel tilt-controlled narrow commuter vehicle." (2006).

[Nakajima 12] Nakajima, Shuro, and Taro Fujikawa. "Proposal for personal mobility vehicle supported by mobility support system." *Electric Vehicle Conference (IEVC), 2012 IEEE International*. IEEE, 2012.

[Nakagawa 13] Nakagawa, Chihiro, et al. "Steering performance of an inverted pendulum vehicle with pedals as a personal mobility vehicle." *Theoretical and Applied Mechanics Letters* 3.1,2013.

[Lie 06] Lie, Anders, et al. "The effectiveness of electronic stability control (ESC) in reducing real life crashes and injuries." *Traffic injury prevention* 7.1: 38-43, 2006.

[Pacejka 05] Pacejka, Hans. *Tire and vehicle dynamics*. Elsevier, 2005..

[Rajamani 11] Rajamani, Rajesh. *Vehicle dynamics and control*. Springer Science & Business Media, 2011.

[Mokhiamar 02] Mokhiamar, O., and Masato Abe. "Active wheel steering and yaw moment control combination to maximize stability as well as vehicle responsiveness during quick lane change for active vehicle handling safety."

Proceedings of the Institution of Mechanical Engineers, Part D: Journal of Automobile Engineering 216.2: 115-124, 2002.

[Hosaka 04] Hosaka, Motoaki, and Toshiyuki Murakami. "Yaw rate control of electric vehicle using steer-by-wire system." *Advanced Motion Control, 2004. AMC'04. The 8th IEEE International Workshop on*. IEEE, 2004.

[Ando 10] Ando, Naoki, and Hiroshi Fujimoto. "Yaw-rate control for electric vehicle with active front/rear steering and driving/braking force distribution of rear wheels." *Advanced Motion Control, 2010 11th IEEE International Workshop on*. IEEE, 2010.

[Kang 11] Kang, Juyong, Jinho Yoo, and Kyongsu Yi. "Driving control algorithm for maneuverability, lateral stability, and rollover prevention of 4WD electric vehicles with independently driven front and rear wheels." *IEEE Transactions on vehicular technology* 60.7: 2987-3001, 2011.

[Harifi 08] Harifi, A., et al. "Designing a sliding mode controller for slip control of antilock brake systems." *Transportation research part C: emerging technologies* 16.6: 731-741, 2008.

[Faragher 12] Faragher, Ramsey. "Understanding the basis of the Kalman filter via a simple and intuitive derivation." *IEEE Signal processing magazine* 29.5: 128-132, 2012.

[Velenis 10] Velenis, Efstathios, Emilio Frazzoli, and Panagiotis Tsiotras. "Steady-state cornering equilibria and stabilisation for a vehicle during extreme operating conditions." *International Journal of Vehicle Autonomous Systems* 8.2-4: 217-241, 2010.

[Chung 06] Chung, Taeyoung, and Kyongsu Yi. "Design and evaluation of side slip angle-based vehicle stability control scheme on a virtual test track." *IEEE*

Transactions on control systems technology 14.2: 224-234, 2006.

[Oufroukh 11] Oufroukh, Naima Ait, et al. "Invariant set based vehicle handling improvement at tire saturation using fuzzy output feedback." *Intelligent Vehicles Symposium (IV), 2011 IEEE*. IEEE, 2011.

초 록

기동성과 횡 안정성을 고려한 역삼륜형 퍼스널 모빌리티 차량의 인휠 모터 제어기 설계

본 논문에서는 역삼륜형 퍼스널 모빌리티 차량의 동역학 모델 분석하였으며 이를 기반으로 기동성 및 횡 안정성 개선을 위한 인휠 모터 제어기를 설계하였다. 퍼스널 모빌리티 차량의 동역학 모델링은 제어기를 설계하기에 앞서 시스템의 성능을 분석하기 위해 설계 및 사용되었다. 특히 모델링을 활용하여 다양한 주행 시나리오 기반으로 시뮬레이션 단계에서 동역학 특성을 검증하였다. 동역학적 특성을 기반으로 목표 요속도를 종 속도에 대한 함수식으로 설계하였다. 목표 요 속도를 추종하기 위한 요 모멘트가 제어기에서 생성되며 본 모멘트를 시스템에 가하여 회전 기동성 및 횡 안정성을 진행 속도에 따라 개선하고자 한다. 목표 요 모멘트는 차분 토크 지령으로 각 모터에 전달되며, 이 외에도 종방향 전복 방지 로직과 바퀴 과도슬립 방지 로직에 의해 각 모터의 토크 지령이 추가 처리된다. Matlab/Simulink를 활용하여 특정 주행 시나리오에서 제어기의 성능을 시뮬레이션 단계에서 검증하였다. 또한 설계된 제어기를 실차에 적용한 뒤 다양한 종 속도, 노면 조건 및 주행 시나리오에 따라 실차 실험이 진행되었다. 실차 실험 결과 저속에서 회전 반경이 급격히 줄어 기동성이 상승되었다. 또한 고속에서는 횡 가속도가 마찰 한계 값 미만으로 제한되어 횡

안정성 역시 확보되었다. 종 방향 전복 방지 및 바퀴 과도 슬립 방지 로직 역시 본 논문에서 설계된 제어기를 통해 성능이 검증되었다.

주요어: Personal Mobility Vehicle, In-Wheel Motor Control, Desired Yaw Rate, Maneuverability, Stability

학 번: 2016-25667